SENSORLESS CONTROL OF PMSM IN LOW SPEED REGION USING HF PULSE SIGNAL INJECTION METHOD

Viktor PETRO, Karol KYSLAN
Department of Electrical Engineering and Mechatronics, Faculty of Electrical Engineering and Informatics,
Technical University of Košice, Letná 9, 042 00 Košice, Slovak Republic, Tel. +421-55-602 2155, E-mail: viktor.petro@tuke.sk

ABSTRACT

The sensorless control of the permanent magnet synchronous motor (PMSM) has attracted wide attention due to its economic and safety benefits. A fast and high-precision rotor-position estimation is necessary for the implementation of sensorless control. In low-speed region, high frequency (HF) signal injection methods are mostly adopted. They suffer to bandwidth deterioration as some digital filters must be included in the current feedback loop or the speed observation signal processing. The HF signal injection method based on the injection of voltage pulses is presented in this paper together with its implementation in MATLAB/Simulink. The method is based on the injection of voltage pulses where injection itself is separated from the motor control algorithm. The simulation results show that the proposed method has good dynamic performance for the sensorless control of PMSM.

Keywords: *permanent magnet synchronous motor, sensorless control, high-frequency pulse signal injection, field-oriented control*

1. INTRODUCTION

Permanent magnet synchronous machines (PMSM) are widely used in the industry due to their high power density, efficiency, and maintenance-free operation. The field-oriented control (FOC) method is utilized for the precise full-speed range control of PMSM. A reliable information about rotor position is essential for the implementation of FOC with PMSM. The information about rotor position is obtained by measurement from resolver or rotary encoder. These sensors are sensitive to electromagnetic noise, require some mounting space, they are relatively expensive and increases the total cost of the drive. Therefore, the research and development of approaches that do not utilize mechanical sensors for position measurement have been provided in recent decades. This approach is mostly referred as a sensorless control. Sensorless control approaches of PMSM can be classified into three major groups, as can be seen in Fig. 1.

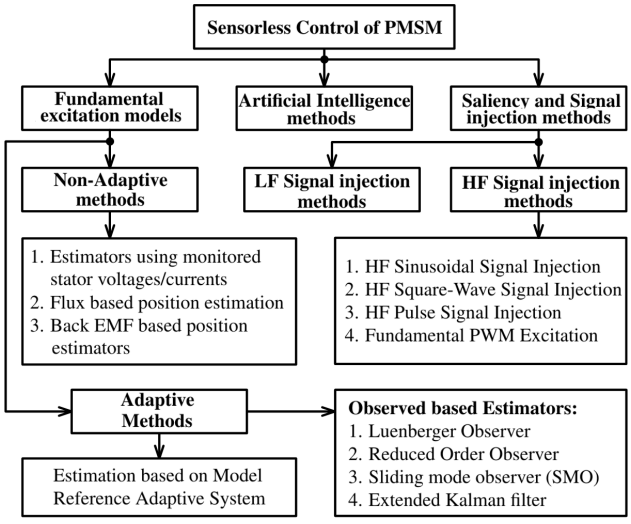

Fig. 1 The overview of methods for sensorless control of PMSM.

The methods based on the fundamental excitation models are well-founded and suitable for medium- and high-speed operation. In most cases the back electromotive force (back-EMF) is utilized in the rotor position and speed observation. Since the amplitude of the back-EMF depends on the motor speed, these approaches fail in position observation at zero and at low-speed ranges where the value of back-EMF has critically low value to be used for reliable position estimation [1].

For low-speed range the magnetic anisotropy of the PMSM needs to be utilized. The anisotropy arises by geometric construction (a saliency of the rotor pole) usually present in the interior permanent magnet synchronous machine (IPMSM) or due to saturation effects in the case of surface-mounted permanent magnet synchronous machine (SMPMSM) [2]. Various high-frequency (HF) injection methods have been developed to utilize the saliency of the PMSM as can be seen in Fig. 1.

In the case of HF sinusoidal signal injection the HF signal is injected in the stator $\alpha\beta$ reference frame: HF rotating sinusoidal signal injection-based method [3], [4], [5], or in the estimated rotor reference frame $\hat{d}\hat{q}$: HF pulsating sinusoidal signal injection-based method [6], [7], [8]. The main drawback of both methods is the upper limit of the injected voltage frequency. The HF waveform of injected voltage must remain sinusoidal what is not fulfilled for the injection of voltages with high frequencies. In addition, digital filters are required to extract signals carrying rotor position information. That restricts the bandwidth of the controllers.

To achieve a higher injection frequency and a better dynamic performance HF square-wave signal injection-based methods were developed [9], [10], [11], [12]. The HF voltage is injected into the estimated rotor reference frame $\hat{d}\hat{q}$ and its shape is a square-wave instead of sinusoidal. The frequency of the injected voltage is a half of the switching frequency. This method does not need digital filtering what helps to increase the bandwidth of controllers and improves the dynamic performance. However, increased losses with this method presents a considerable disadvantage [13].

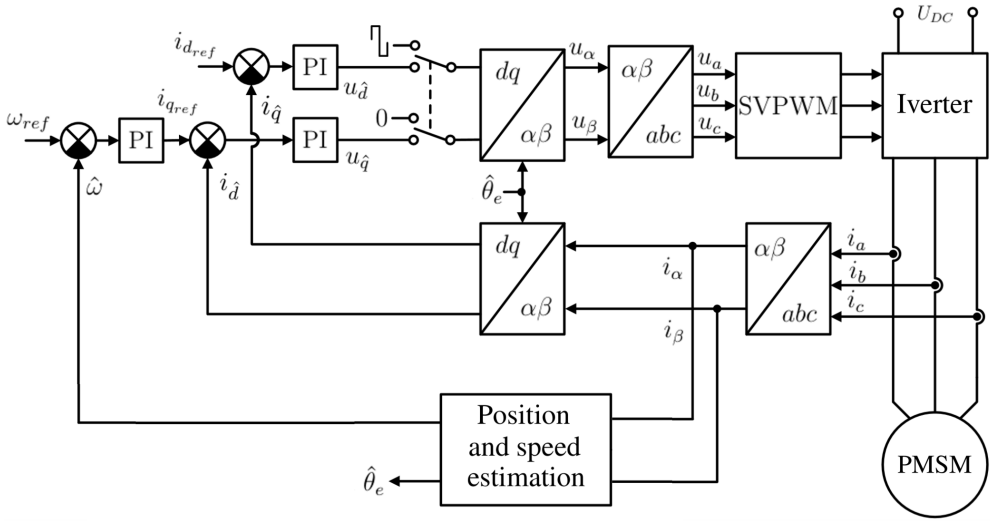

Fig. 2 The block diagram of the sensorless control of PMSM using the HF pulse signal injection method.

The position and the speed estimation error can be also negatively affected by the inverter nonlinearities and voltage drops. HF pulse signal injection-based method [13], [14] was introduced in recent years to overcome all specified drawbacks of previous methods. The main idea of this method is that HF pulse signal is injected while the FOC algorithm is interrupted. It means that the separate periods are used for the FOC and for the signal injection. The main advantage of this approach is that the fundamental frequency current is separated from the HF component and no digital filters are required, either in the estimation process or in the feedback for current regulators. The robustness against voltage errors caused by the inverted nonlinearities is also improved. This approach is used in this paper.

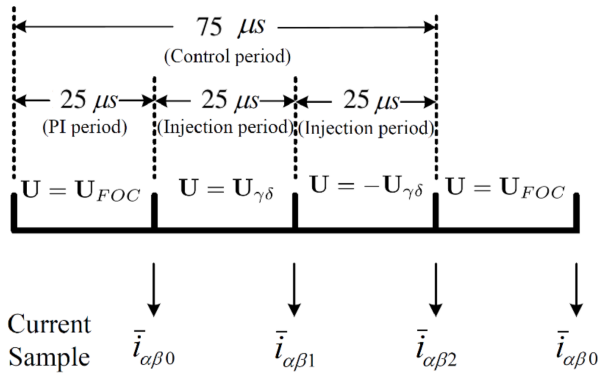

Fig. 3 The three switching periods during one control period.

2. HIGH FREQUENCY PULSE SIGNAL INJECTION BASED METHOD

The block diagram of the HF pulse signal injection-based method implemented in sensorless control of PMSM is shown Fig. 2. A switch is used to represent the fact, that either the FOC is executed or the HF pulse voltage is injected. The overall control period contains three switching periods as in Fig. 3. The switching period is set to 40 kHz (25 μs) and the overall control period is 13.33 kHz (75 μs). In the first period, the FOC routine is executed and current PI controllers in the control structure create the applied voltage vector in the three phase stator reference frame **U**. In the following two periods, the positive and negative pulse voltages are injected, while the algorithm of the FOC is interrupted (i.e. not executed). The injected voltage is applied in the estimated $\hat{d}\hat{q}$ axis, often referred to as the $\gamma\delta$ reference frame. The injection can be performed either in the estimated $\hat{d}$ (γ) or $\hat{q}$ (δ) axis. Usually the estimated $\hat{d}$ (γ) is preferred since the torque ripples caused by the HF voltage injection are then minimized. The relationship between the true and estimated rotor reference frame, dq and $\hat{d}\hat{q}$ ($\gamma\delta$) can be seen in Fig. 4.

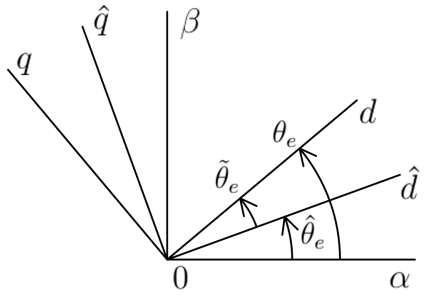

Fig. 4 The real and estimated reference systems.

The currents are measured at the beginning of each switching period, as can be seen in Fig. 3. The following stands for the current variation in the $\alpha\beta$ reference frame [14]:

$$\Delta\mathbf{i}_{\alpha\beta} = (c_1 + c_2 e^{j2(\theta_e-\theta_u)})\mathbf{u}_{\alpha\beta}\Delta T, \tag{1}$$

where $c_1 = \frac{\Sigma L}{\Sigma L^2+\Delta L^2}$, $c_2 = \frac{-\Delta L}{\Sigma L^2+\Delta L^2}$, where $\Sigma L = \frac{L_d+L_q}{2}$, $\Delta L = \frac{L_d-L_q}{2}$ and L_d, L_q are the direct and quadrature axis inductances respectively, θ_e is the actual electrical rotor position, θ_u is the angle of the applied voltage vector in the $\alpha\beta$ reference frame and $\mathbf{u}_{\alpha\beta} = U_m e^{j\theta_u}$, where U_m is the amplitude of the voltage vector $\mathbf{u}_{\alpha\beta}$. As the pulse voltage is injected in the estimated $\hat{d}\hat{q}$ ($\gamma\delta$) axis, it is convenient to transform (1) into the estimated rotor reference frame. For this purpose, the estimated rotor position $\hat{\theta}_e$ is introduced [14]:

$$\Delta\mathbf{i}_{\gamma\delta} = \Delta\mathbf{i}_{\alpha\beta} e^{-j\hat{\theta}_e} = (c_1 + c_2 e^{j2(\theta_e-\hat{\theta}_e-\hat{\theta}_u)})\mathbf{u}_{\gamma\delta}\Delta T, \tag{2}$$

where $\mathbf{u}_{\gamma\delta}$ is the voltage vector represented in the estimated $\hat{d}\hat{q}$ ($\gamma\delta$) axis and $\hat{\theta}_u = \theta_u - \theta_e$ is the voltage angle in the estimated reference frame and ΔT is the duration of one switching period. The d axis current component does not produce any torque in the machine and the injection is applied in the observed $\hat{d}$ (γ) axis. Following holds for the positive and negative injected pulse voltages:

$$\begin{aligned}\mathbf{u}_{\gamma\delta 1} &= U_m e^{j\hat{\theta}_{u1}} \approx U_m e^{j0} - \Delta\mathbf{u},\\ \mathbf{u}_{\gamma\delta 2} &= U_m e^{j\hat{\theta}_{u2}} \approx U_m e^{j\pi} - \Delta\mathbf{u},\end{aligned} \tag{3}$$

where $\mathbf{u}_{\gamma\delta 1}, \mathbf{u}_{\gamma\delta 2}$ denotes the first and second injected pulse voltage, respectively, $\hat{\theta}_{u1}, \hat{\theta}_{u2}$ are the injected voltage angles in the estimated $\hat{d}\hat{q}$ ($\gamma\delta$) reference frame and $\Delta\mathbf{u}$ is the inverter voltage error caused by nonlinearities. Substituting (3) into (2) leads to:

$$\begin{aligned}\Delta\mathbf{i}_{\gamma\delta 1} &= \Delta T c_1 (U_m e^{j0} - \Delta\mathbf{u}) + \Delta T c_2 e^{j2\tilde{\theta}_e} e^{-j\hat{\theta}_{u1}} U_m,\\ \Delta\mathbf{i}_{\gamma\delta 2} &= \Delta T c_1 (U_m e^{j\pi} - \Delta\mathbf{u}) + \Delta T c_2 e^{j2\tilde{\theta}_e} e^{-j\hat{\theta}_{u2}} U_m,\end{aligned} \tag{4}$$

where $\tilde{\theta}_e = \theta_e - \hat{\theta}_e$ is the rotor position observation error. Since the injection is provided in the real axis, the position error can be linked to the imaginary part of the current variations as follows:

$$\mathrm{Im}(\Delta\mathbf{i}_{\gamma\delta 1} - \Delta\mathbf{i}_{\gamma\delta 2}) = 2k\sin(2\tilde{\theta}_e) \approx 4k\tilde{\theta}_e, \tag{5}$$

where $k = \Delta T c_2 U_m$ and for the imaginary part of the current differences $\Delta\mathbf{i}_{\gamma\delta 1}$, $\Delta\mathbf{i}_{\gamma\delta 2}$ stands:

$$\begin{aligned}\mathrm{Im}(\Delta\mathbf{i}_{\gamma\delta 1}) &= -(i_{\alpha 1} - i_{\alpha 0})\sin\hat{\theta}_e + (i_{\beta 1} - i_{\beta 0})\cos\hat{\theta}_e,\\ \mathrm{Im}(\Delta\mathbf{i}_{\gamma\delta 2}) &= -(i_{\alpha 2} - i_{\alpha 1})\sin\hat{\theta}_e + (i_{\beta 2} - i_{\beta 1})\cos\hat{\theta}_e.\end{aligned} \tag{6}$$

The estimated rotor position $\hat{\theta}_e$ and speed $\hat{\omega}_e$ can be obtained using a phase-lock loop (PLL) according to Fig. 5 [15]. First, the current variations in $\alpha\beta$ reference frame are calculated during the two injection periods. Next, the Park transformation is used to transform the current derivations into the observed rotor reference frame $\hat{d}\hat{q}$ ($\gamma\delta$). During the transformation, the observed rotor position $\hat{\theta}_e$ is used. Only the imaginary part of the current derivation contains the rotor position observation error $\tilde{\theta}_e$, and so this part is extracted further. These three steps are all included in (6). If $\tilde{\theta}_e$ is regulated to the zero value, the observed position and speed will converge to the real values and the estimated $\hat{d}\hat{q}$ ($\gamma\delta$) reference frame will align to the real dq reference frame.

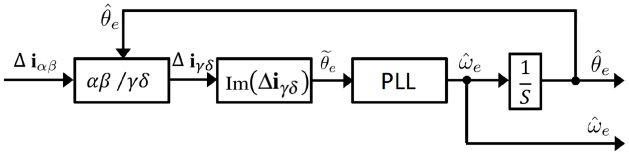

Fig. 5 The coordinate transformation and PLL used for position and rotor speed observation in HF pulse signal injection [14].

Table 1 PMSM parameters used in the simulation.

parameter	notation	value
DC voltage	v_{DC}	230 V
nominal torque	T_N	2.44 Nm
nominal current	i_N	3 A
torque constant	k_t	0.813 Nm/A
nb. of pole-pairs	$2p$	2
nominal speed	n_N	3800 rpm
resistance	R_{ab}	6.98 Ω
d-axis inductance	L_d	0.012 mH
q-axis inductance	L_q	0.034 mH
total inertia	J	0.005 kg.m^2
viscous friction	B	0.0008 Nms/rad
PLL P-component	k_P	10 000
PLL I-component	k_I	1 800 000

3. SIMULATION RESULTS

The simulations were performed and analysed with MATLAB/Simulink environment. The interior PMSM with the significant rotor inductions saliency was chosen to be simulated and the switching frequency was set to 40 kHz. The motor parameters are listed in Tab. 1.

Two different amplitudes U_m = 40 V and U_m = 10 V were selected to analyze the influence of the injected voltage amplitude on the estimation performance. The simulation results for U_m = 40 V are shown in Fig. 6 and for U_m = 10 V in Fig. 7. The layout of the figures is the following: up left: the estimated, actual and reference speed, up right: the error in speed observation, middle left: the estimated and actual electrical rotor position, middle right: the error in rotor position observation, bottom left: the direct and quadrature axis currents i_d and i_q, bottom right the two-axis stator current components i_α and i_β. The step reference speed was set to $\omega_{ref} = 15$ rad/s (143 rpm). During the transient state, the maximum rotor position observation

error $\Delta\theta_e$ for U_m = 40 V was about 0.006 rad (0.34 electrical degrees) and for U_m = 10 V was about 0.031 rad (1.78 electrical degrees). The maximum speed error was around 0.5 rad/s (5 rpm) for U_m = 40 V and 1.8 rad/s (17 rpm) for U_m = 10 V. At time t = 0.4 s the motor was loaded with nominal torque and at time t = 0.8 s the motor was unloaded.

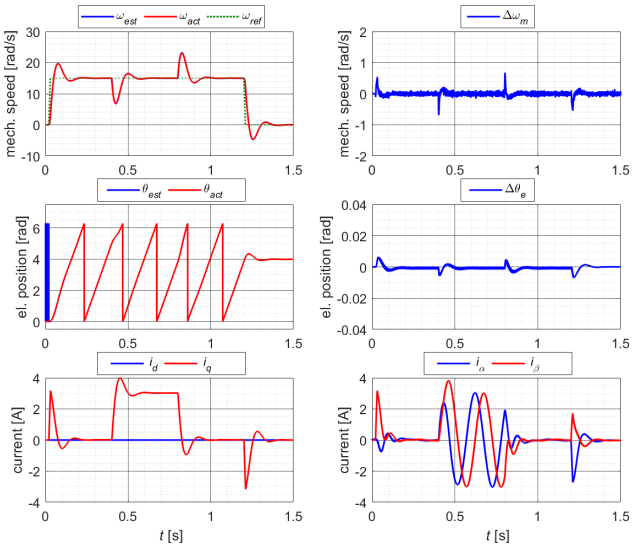

Fig. 6 The simulation results of sensorless control with HF pulse signal injection method for U_m = 40 V.

As can be seen from Fig. 6 and Fig. 7 during the transient states of loading and unloading the motor, the observation error increases but the observed values converge very fast to the real values. It can be stated that observation and sensorless control of the PMSM has a satisfactory robustness and dynamic performance. The currents shown in Fig. 6 and Fig. 7 are measured only during the FOC period.

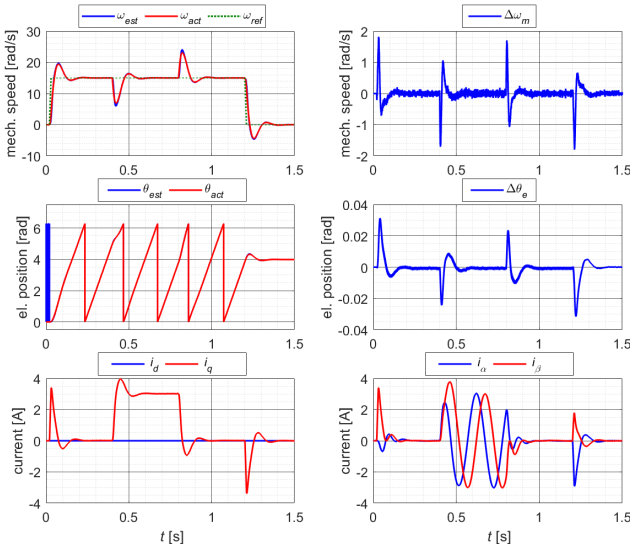

Fig. 7 The simulation results of sensorless control with HF pulse signal injection method for U_m = 10 V.

Therefore, no HF current components are visible in the current waveforms. It is the main benefit of this approach since no low-pass filters (DPF) are required in the current loop feedbacks. The real phase currents i_a, i_b, and i_c are shown in the top of Fig. 8. A detail of the real phase current i_a can be seen in the middle of Fig. 8 (in blue colour). It is clear that the injection of the HF voltages induces HF current components in phase currents. But since the currents for the current regulators feedback are used only during the FOC period when no HF voltage injection is performed, the measured currents seem to be smooth without any HF components superimposed onto the current waveform, as can be seen in the middle of Fig. 8 (in red colour). A more detailed comparison of the real phase current i_a and the sample of this current used as feedback for the current regulators i_{afb} can be seen in the bottom of the figure.

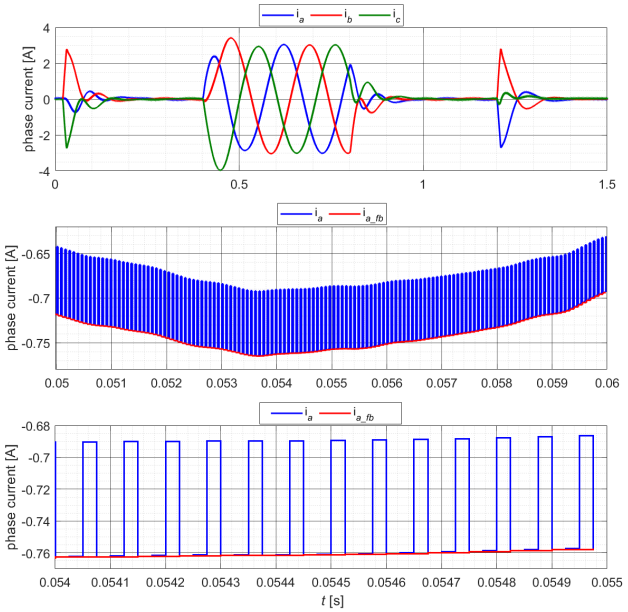

Fig. 8 top: phase currents i_a, i_b and i_c, middle: a detail of current i_a and the current used for feedback i_{a_fb}, bottom: expanded detail of i_a and i_{a_fb}.

It should be noted that even if the overall control period consists of three switching periods (see Fig. 3) and the FOC is calculated only once per control period, the frequency of the execution of FOC is 3-times lower than switching frequency. It means that the currents are sampled with a frequency of 40 kHz but the FOC is executed only at 13.33 kHz. This might cause some deterioration of performance in the lower current sampling frequency regions. Although nowadays the switching frequency of 40 kHz can be easily achieved without using special high-end microcontrollers.

The main part of the MATLAB/Simulink model can be seen in Fig. 9. The FOC is executed only if the trigger signal falls. The trigger signal falls to the value of 0 at the beginning of each FOC period in Fig. 3.

In this case, the bottom input is connected to the switch

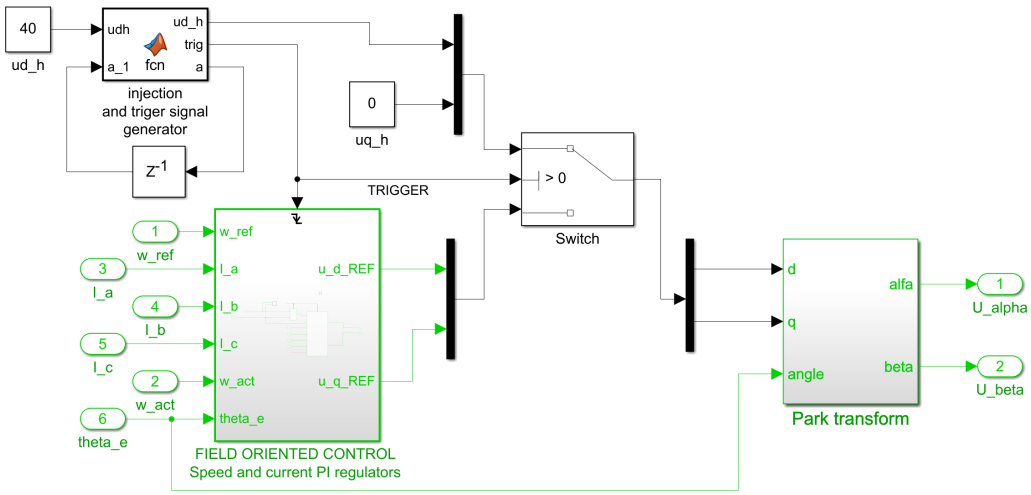

Fig. 9 Simulink implementation of different switching periods for HF pulse injection method, injection of pulse is separated from field-oriented control.

output in Fig. 9. It means that the reference voltages u_{d_ref}, u_{q_ref} enter the Park transformation and further they are used to energize the motor windings.

In the following switching period the trigger signal rises from zero to the value of 1 and remains the same value also during the third period, until the begging of the next FOC period occurs. While the trigger is a non-zero value, the top input is connected to the switch output in Fig. 9. In this case the quadrature axis voltage is held to zero: $u_{qh} = 0$ V while the direct axis voltage is set to $u_{dh} = U_m$ or $u_{dh} = -U_m$ according to the actual injection period. This implementation allows a separation of the field-oriented control algorithm and the HF signal injection what brings many benefits.

4. CONCLUSIONS

Sensorless control of PMSM using HF pulse signal injection method and its implementation was described in this paper. By the separation of HF injection from the algorithm of field-oriented control, the low-pass filters are not necessary and the bandwidth of the current controllers is not affected. It results in very good dynamic performance of the sensorless algorithm. Simulation results show that such modification of sensorless control has a good performance and observation ability during steady states and transient operation. The described algorithm is suitable for sensorless control of PMSM machine in low- and very-low speed regions and it is quite simple to implement, making it a serious competitor against commonly known sensorless approaches.

ACKNOWLEDGEMENT

This work was supported by the Scientific Grant Agency of the Ministry of Education of the Slovak Republic under the project VEGA 1/0493/19. This work was also supported by Faculty of Electrical Engineering and Informatics, Technical University of Košice, Slovakia, under Grant FEI-2022-86 *Experimentalne overenie bezsnimačoveho riadenia SMPM s integrovanym meničom.*

REFERENCES

[1] PETRO, V. – KYSLAN, K.: ”Design and Simulation of Direct and In-direct Back EMF Sliding Mode Observer for Sensorless Control of PMSM”, Power Electronics and Drives. 2020; 5(1):215-228. https://doi.org/10.2478/pead-2020-0016.

[2] SCHROEDL, M.: ”Sensorless control of ac machines at low speed and standstill based on the INFORM method”, in IAS 1996. Conference Record of the 1996 IEEE Industry Applications Conference Thirty-First IAS Annual Meeting, vol. 1, 1996, pp. 270-277 vol.1.

[3] JANSEN, P. – LORENZ, R.: ”Transducerless position and velocity estimation in induction and salient ac machines”, IEEE Transactions on Industry Applications, vol. 31, no. 2, pp. 240-247, 1995.

[4] CILIA, J. – ASHER, G. – BRADLEY, K.: ”Sensorless position detection for vector controlled induction motor drives using an asymmetric outer-section cage”, in IAS 1996. Conference Record of the 1996 IEEE Industry Applications Conference Thirty-First IAS Annual Meeting, vol. 1, 1996, pp. 286-292 vol.1.

[5] G. WANG, G. – VALLA, M. – SOLSONA, J.: ”Position sensorless permanent magnet synchronous machine drives a review”, IEEE Transactions on Industrial Electronics, vol. 67, no. 7, pp. 5830-5842, 2020.

[6] CORLEY, M. – LORENZ, R.: ”Rotor position and velocity estimation for a permanent magnet synchronous machine at standstill and high speeds”, in IAS 1996. Conference Record of the 1996 IEEE Industry Applications Conference Thirty-First IAS Annual Meeting, vol. 1, 1996, pp. 36-41 vol.1.

[7] JANG, J.-H. – SUL, S.-K. – HA, J.-I. – IDE, K. – SAWAMURA, M.: ”Sensorless drive of surface-mounted permanent-magnet motor by high-frequency signal injection based on magnetic saliency”, IEEE Transactions on Industry Applications, vol. 39, no. 4, pp. 1031-1039, 2003.

[8] BIANCHI, N. – BOLOGNANI, S. – JANG, J.-H. – SUL, S.-K.: "Advantages of inset pm machines for zero-speed sensorless position detection", in Conference Record of the 2006 IEEE Industry Applications Conference Forty-First IAS Annual Meeting, vol. 1, 2006, pp. 495-502.

[9] MASAKI, R. – KANEKO, S. – HOMBU, M. – SAWADA, T. – YOSHIHARA, S.: "Development of a position sensorless control system on an electric vehicle driven by a permanent magnet synchronous motor", in Proceedings of the Power Conversion Conference-Osaka 2002 (Cat. No.02TH8579), vol. 2, 2002, pp. 571-576 vol.2.

[10] KIM, D. – KWON, Y.-C. – SUL, S.-K. – KIM, J.-H. – YU, R.-S.: "Suppression of injection voltage disturbance for high-frequency square-wave injection sensorless drive with regulation of induced high-frequency current ripple", IEEE Transactions on Industry Applications, vol. 52, no. 1, pp. 302-312, 2016.

[11] NI, R. – LU, K. – BLAABJERG, F. – XU, D.: "A comparative study on pulse sinusoidal high frequency voltage injection and inform methods for pmsm position sensorless control", in IECON 2016 - 42nd Annual Conference of the IEEE Industrial Electronics Society, 2016, pp. 2600-2605.

[12] LIU, J. – ZHANG, Y. – YANG, H. – SHEN, W.: "Position sensorless control of pmsm drives based on hf sinusoidal pulsating voltage injection", in 2020 IEEE Energy Conversion Congress and Exposition (ECCE), 2020, pp. 3849-3853.

[13] WANG, G. – ZHANG, G. – XU, D.: "Position Sensorless Control Techniques for Permanent Magnet Synchronous Machine Drives", Springer Nature Singapore Pte Ltd. 2020, 2020, ISBN 978-981-15-0049-7

[14] XIE, G. – LU, K. – DWIVEDI, S.-K. – ROSHOLM, J. R. – BLAABJERG, F.: "Minimum-voltage vector injection method for sensorless control of pmsm for low-speed operations", IEEE Transactions on Power Electronics, vol. 31, no. 2, pp. 1785-1794, 2016.

[15] WANG, G. – LI, Z. – ZHANG, G. – YU, Y. – XU, D.: "Quadrature pll-based high-order sliding-mode observer for ipmsm sensorless control with online mtpa control strategy", IEEE Transactions on Energy Conversion, vol. 28, no. 1, pp. 214-224, 2013.

Received March 18, 2022, accepted April 21, 2022

BIOGRAPHIES

Viktor Petro received the B.Sc. and M.Sc. degrees in electrical engineering from Technical University of Košice, Slovakia, in 2018 and 2020, respectively. He is currently working towards a Ph.D. degree with the Technical University of Košice at the Department of Electrical Engineering and Mechatronics. His research interest is control of electrical drives with a focus on position-sensorless control of permanent magnet synchronous motors based on injection methods.

Karol Kyslan received M.Sc. and Ph.D. degrees in electrical engineering from the Technical University of Košice, Slovak Republic, in 2009 and 2012; respectively, and the habilitation degree in electrical drives from the same university in 2020. He is currently an Associate Professor with the Department of Electrical Engineering and Mechatronics, Technical University of Košice, Slovakia, teaching courses on electrical drives. His research interests include control of electrical drives and motion control, finite control set model predictive control, sensorless control and hardware-in-the-loop systems. He is a member of IEEE.